12
Terbium(III) Footprinting as a Probe of RNA Structure and Metal-binding Sites

Dinari A. Harris and Nils G. Walter

12.1
Introduction

Cations play a pivotal role in RNA structure and function. A functional RNA tertiary structure is stabilized by metal ions that neutralize and, in the case of multivalents, bridge the negatively charged phosphoribose backbone [1]. The current chapter describes the use of the trivalent lanthanide metal ion terbium(III) as a versatile probe of high-affinity metal ion binding sites, as well as of RNA secondary and tertiary structure. Terbium(III) has a similar ion radius (0.92 Å) as magnesium(II) (0.72 Å) and a similar preference for oxygen and nitrogen ligands over softer ones. Thus, terbium(III) binds to similar sites on RNA as magnesium(II); however, with 2–4 orders of magnitude higher affinity. Unlike magnesium(II), the low pK_a of the aqueous terbium(III) complex (around 7.9) generates enough $Tb(OH)_{(aq)}^{2+}$ to make it capable of hydrolyzing the RNA backbone around neutral pH via deprotonation of the 2′-hydroxyl group and nucleophilic attack of the resulting oxyanion on the adjacent 3′,5′-phosphodiester to form 2′,3′-cyclic phosphate and 5′-hydroxyl termini [2]. Under physiological conditions, therefore, low (micromolar) concentrations of Tb^{3+} ions readily displace medium (millimolar) concentrations of Mg^{2+} ions from high-affinity binding sites (both specific and nonspecific ones) and promote slow phosphodiester backbone cleavage, revealing their location on the RNA. Higher (millimolar) concentrations of Tb^{3+} ions bind less specifically to RNA and result in backbone cleavage in a sequence-independent manner, preferentially cutting solvent accessible, single-stranded or non-Watson–Crick base-paired regions, thus providing a footprint of the RNA's secondary and tertiary structure at nucleotide resolution.

Terbium(III) can be a very straightforward and useful probe of metal binding and tertiary structure formation in RNA. However, there are several precautions that need to be considered in order to obtain a reliable and reproducible RNA footprinting pattern. Since low (micromolar) concentrations of terbium(III) bind to high-affinity metal binding sites within a folded RNA, while high (millimolar) concentrations produce a footprinting pattern of solvent accessible regions, it is critical to perform terbium(III) induced cleavage reactions over a wide range of Tb^{3+} con-

Handbook of RNA Biochemistry. Edited by R. K. Hartmann, A. Bindereif, A. Schön, E. Westhof

ISBN: 3-527-30826-1

centrations. To ensure conformational homogeneity, pre-folding the RNA under optimized buffer conditions and magnesium concentrations is necessary. This is especially important when trying to identify metal-binding sites, since there will be relatively few cleavage events at low Tb^{3+} concentrations. All cleavage reactions should be performed near physiological pH (7.0–7.5) to allow for the accumulation of the cleavage active $Tb(OH)_{(aq)}^{2+}$ species [3]. Insoluble polynuclear hydroxo aggregates of terbium(III) can form at pH 7.5 and above [4, 5], which should be avoided. Another parameter that needs to be empirically optimized is the temperature and duration of the metal-ion-induced cleavage reactions. Higher temperatures result in faster cleavage rates, but also increase the amount of background degradation. Therefore, typical reaction temperatures range from 25 to 45 °C over a period of 0.5–2 h. All of these parameters need to be well established prior to carrying out terbium(III) footprinting experiments in earnest.

12.2
Protocol Description

12.2.1
Materials

Reagents and buffers

Appropriate buffers to fold RNA (usually Tris, MES and/or HEPES of desired pH)
1 M $MgCl_2$ solution.
100 mM $TbCl_3$ in 5 mM sodium cacodylate buffer, pH 5.5 (store in small aliquots at −20 °C).
0.5 M Na_2EDTA, pH 8.0.
Urea loading buffer: 8 M urea, 50 mM EDTA, pH 8.0, 0.01% bromophenol blue, 0.01% xylene cyanol.

Equipment

Heating block at 90 °C.
Water bath.
Phosphor screens and phosphorImager with appropriate software [e.g. PhosphorImager Storm 840 with ImageQuant software (Molecular Dynamics)].

(1) Prior to performing terbium(III) mediated footprinting of an RNA molecule, the RNA should be end-labeled (typically with ^{32}P at either the 5′ or 3′ end), purified by denaturing gel electrophoresis, and stored in water (or an appropriate buffer) at −20 °C.
(2) Prepare a single pool with 250 000–500 000 c.p.m. (typically 0.5–2 pmol) of end-labeled RNA per reaction aliquot under appropriate buffer conditions and heat denature at 90 °C for 2 min. The total pool volume should be sufficient for single or duplicate reaction aliquots at each desired Tb^{3+} concentration.

(3) Pre-fold the RNA, by incubating the pool at an optimized temperature (typically 25–45 °C) for approximately 10 min to ensure structural homogeneity. Some RNAs fold best when a slow-cooling procedure is used or when certain cations are already added at this stage.

(4) To obtain the desired Mg^{2+} concentration, add an aliquot of $MgCl_2$ from an appropriately diluted stock solution and equilibrate at the optimized temperature for an additional 5–10 min. At this point, the total volume of the reaction mixture should be 8 µl per reaction aliquot.

(5) From the 100 mM $TbCl_3$ stock solution, make a serial set of $TbCl_3$ dilutions in water, ranging from micromolar to millimolar concentrations (5× over the final reaction concentration). This wide range of $TbCl_3$ concentrations should be sufficient to probe for both high-affinity metal binding sites and secondary/tertiary structure formation. *Note: The 100 mM $TbCl_3$ stock solution is dissolved in a 5 mM sodium cacodylate buffer at pH 5.5 to prevent formation of terbium(III) hydroxide precipitates at higher pH. The $TbCl_3$ dilutions in water should be made immediately prior to use. A serial set of dilutions is recommended to ensure consistency in cleavage band intensity between gel lanes. Use a fresh aliquot of 100 mM $TbCl_3$ stock solution each time. Final $TbCl_3$ concentrations used in the cleavage reactions should be optimized together with other experimental conditions for the specific RNA and experimental goal.*

(6) To initiate terbium(III) mediated cleavage, mix an 8-µl aliquot from the pool containing the end-labeled RNA, buffer components and Mg^{2+} with 2 µl of an appropriate dilution of $TbCl_3$ to achieve the desired final Tb^{3+} concentration (typically ranging from 5 µM to 5 mM , in addition to a 0 mM Tb^{3+} control). Continue to incubate at the optimized temperature for an optimized amount of time (typically 30 min to 2 h). *Note*: The incubation times should be chosen to generate a partial digestion pattern of end-labeled RNA under single-hit conditions. Extended incubation times will increase secondary hits that may reflect structural distortions of the RNA.

(7) Quench the cleavage reaction by adding EDTA, pH 8.0, to a final concentration of 50 mM (or at least a 2-fold excess over the total concentration of multivalent metal ions in the reaction aliquot).

(8) Perform an ethanol precipitation of the RNA by adding Na(OAc) to a final concentration of 0.3 M and 2–2.5 volumes of 100% ethanol, and precipitate at −20 °C overnight. Centrifuge 30 min at 12 000 *g*, 4 °C. Decant supernatant, wash with 80% ethanol, decant supernatant, and dry RNA in a Speed Vac evaporator. Re-dissolve samples in 10–20 µl of urea loading buffer.

(9) Partial alkaline hydrolysis and RNase T1 digestion reactions of the same RNA should be performed as calibration standards by incubating the end-labeled RNA in the appropriate buffers.

(10) Heat samples at 90 °C for 5 min and place on ice water to snap cool. Analyze the cleavage products on a high-resolution denaturing (8 M urea) polyacrylamide sequencing gel, using the partial alkaline hydrolysis and RNase T1 digestion reactions as size markers to identify the specific terbium(III) cleavage products at nucleotide resolution. *Note: In the example cited below, a wedged,*

8 M urea, 20% polyacrylamide *gel was run at a constant power of 80 W for separating the reaction products of a radiolabeled 39mer RNA. Identical samples can be loaded at different times on the same gel to resolve different regions of longer RNA.*

(11) Product bands are directly visualized by exposing the gel to a phosphor screen. *Note: The exposure can take several hours to overnight, depending on the level of radioactivity of the bands in the gel.*

(12) Quantify the full-length RNA and cleavage product bands using a volume count method. (For a more qualitative evaluation, a line scan method can be used.) At every Tb^{3+} concentration, calculate a normalized extent of cleavage (Π) by substituting the peak intensities in the equation:

$$\Pi = \frac{\left(\dfrac{\text{band intensity at nucleotide } x}{\sum_i \text{band intensity at nucleotide } i}\right)_{y[Tb^{3+}]}}{\left(\dfrac{\text{band intensity at nucleotide } x}{\sum_i \text{band intensity at nucleotide } i}\right)_{0\ \text{mM}\ [Tb^{3+}]}}$$

where y is the terbium(III) concentration in a particular cleavage reaction and x the analyzed nucleotide position of the RNA. 0 mM [Tb^{3+}] signifies a control reaction incubated in the same fashion as the terbium(III) containing ones except that no terbium(III) is added. A Π value of ≥ 2 indicates significant cleavage over background degradation. *Note: By dividing the ratio of a*

Fig. 12.1. Terbium(III) footprinting of the *trans*-acting HDV ribozyme. (A) Synthetic HDV ribozyme construct D1. The ribozyme portion is shown in bold, and consists of two separate RNA strands A and B. 3′ Product (3′P) is shown outlined. The substrate variant S3 contains eight additional nucleotides (gray) 5′ of the cleavage site (arrow). To generate non-cleavable substrate analogs, the 2′-OH of the underlined nucleotide immediately 5′ of the cleavage site was modified to 2′-methoxy and the suffix "nc" added to their name. Dashed lines, tertiary structure hydrogen bonds of C75 and the ribose zipper of A77 and A78 in joiner J4/2. (B) Terbium(III)- and magnesium(II)-mediated footprint of the 5′-^{32}P-labeled HDV ribozyme strand A upon incubation with terbium(III) for 2 h in 40 mM Tris–HCl, pH 7.5, 11 mM $MgCl_2$ at 25 °C. From left to right as indicated: strand A fresh after radiolabeling; incubated in buffer without Tb^{3+}; incubated with excess strand B in buffer without Tb^{3+}; incubated in buffer without Tb^{3+}; incubated with excess strand B and non-cleavable substrate analog ncS3 in buffer without Tb^{3+}; RNase T1 digest; alkali (OH^-) ladder; footprint with increasing Tb^{3+} concentrations in the presence of excess strand B and ncS3; incubated in buffer without Tb^{3+}; incubated with excess strand B in buffer without Tb^{3+}; footprint with increasing Tb^{3+} concentrations in the presence of excess strand B and 3′ product (3′P). As the terbium(III) concentration increases, backbone scission becomes more intense. The 5′ and 3′ segments of P1.1 (boxed) footprint very differently in the precursor and product complexes. Far right, magnesium(II)-induced cleavage at pH 9.5 and 37 °C, for comparison; from left to right: precursor (ncS3) complex, control incubated at pH 7.5; precursor complex, footprinted at pH 9.5; product complex, control incubated at pH 7.5; product complex, footprinted at pH 9.5. Reprinted with permission from [6].

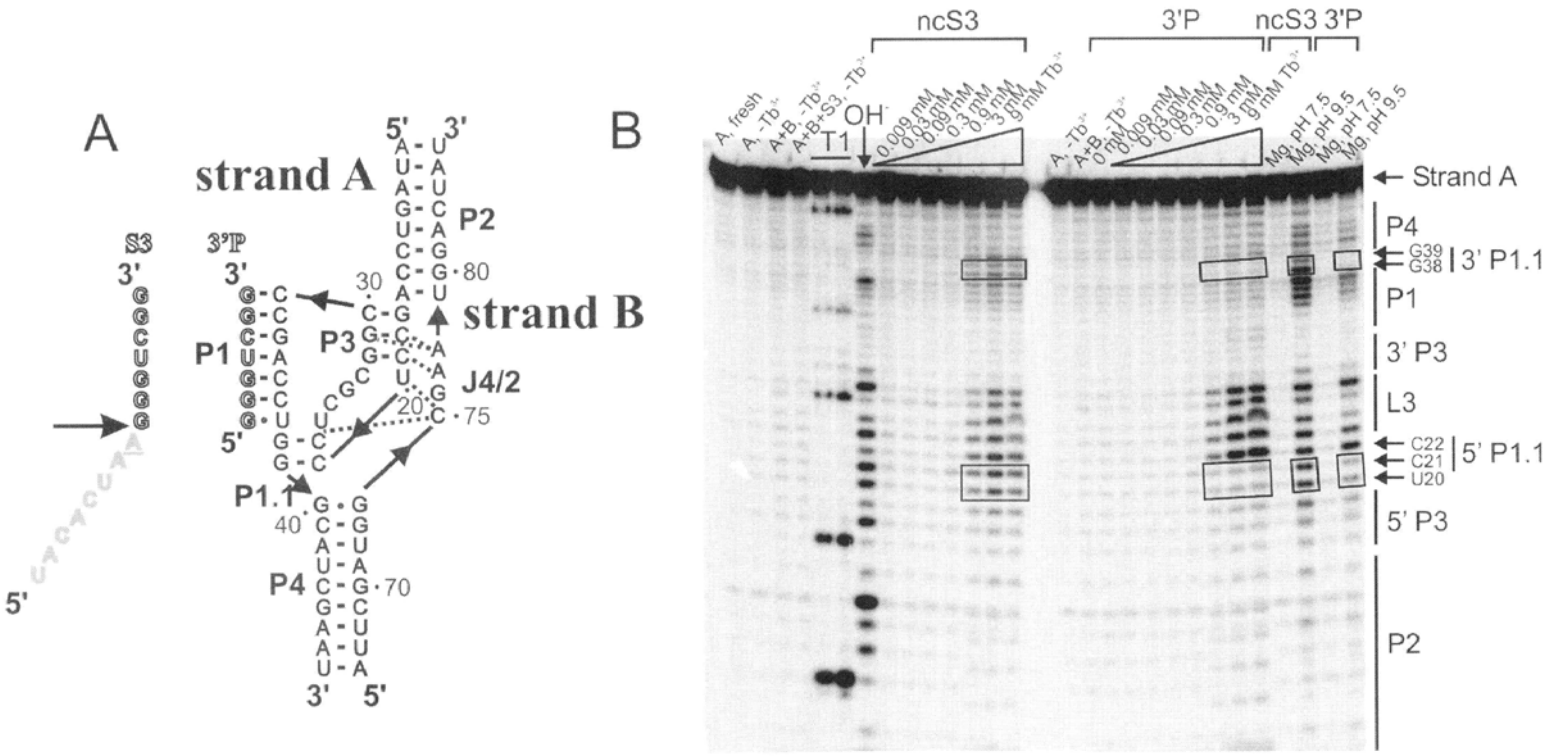
A
strand A
strand B
S3
3'P
P1
P1.1
P2
P3
P4
J4/2
5'
3'
B
ncS3
3'P
OH-
T1
Strand A
P4
G39
G38
3' P1.1
P1
3' P3
L3
C22
C21
U20
5' P1.1
5' P3
P2

Fig. 12.1

single band intensity over total RNA in the presence of terbium(III) by the ratio of a single band intensity over total RNA in the absence of terbium(III), one normalizes for the effect of non-specific background degradation.

12.3 Application Example

Terbium(III) has been successfully used on a number of RNAs as probe for high-affinity metal-binding sites and tertiary structure formation. For example, taking advantage of its luminescent, as well as RNA footprinting properties, terbium(III) has recently revealed subtle structural differences between the precursor and product forms of the hepatitis delta virus (HDV) ribozyme [6]. The HDV ribozyme is a unique RNA motif found in the human HDV, a satellite of the hepatitis B virus that leads to frequent progression towards liver cirrhosis in millions of patients worldwide [7]. There is a strong interest, both for medical and fundamental reasons, in understanding structure and function relationships in this catalytic RNA. We found that the terbium(III) mediated footprinting pattern of the 3′ product (3′P) complex of a *trans*-acting version of the HDV ribozyme (Fig. 12.1A), obtained in the presence of millimolar Tb^{3+} concentrations, is consistent with a post-cleavage crystal structure. In particular, protection is observed in all five Watson–Crick base-paired stems, P1 through P4 and P1.1, while the backbone of the L3 loop region and that of the J4/2 joining segment are strongly cut (Fig. 12.1) [6]. Cuts in the J4/2 joiner are particularly relevant since it encompasses the catalytic residue C75 and its neighboring G76, and the strong terbium(III) hits implicate it as a region of high negative charge density with high affinity for metal ions.

Strikingly, terbium(III) footprinting reveals the precursor (ncS3) structure as distinct; while P1, P2, P3 and P4 remain protected, both the 5′ and 3′ segments of the P1.1 stem (as well as U20, immediately upstream) are strongly hit, suggesting that this helix in the catalytic core is formed to a lesser extent than in the product complex. In addition, scission in J4/2 extends to A77 and A78, implying that the ribose zipper motif involving these nucleotides may not be fully formed in the precursor complex (Fig. 12.1B). These differences in extent of backbone scission in the precursor versus the 3′ product complexes show that a significant conformational

Fig. 12.2. Sites of backbone scission mediated by 3 mM terbium(III) in 40 mM Tris–HCl, pH 7.5, 11 mM $MgCl_2$ at 25 °C and superimposed onto two-dimensional representations of the precursor and product HDV ribozyme secondary structures. Only the catalytic core residues are explicitly shown. Relative scission intensities were calculated as described in Section 12.2 and are represented by the symbol code. Scission is located 3′ of the indicated nucleotides. Only the product structure is likely to fully form P1.1 and the ribose zipper of A77 and A78 in J4/2, as suggested by solid and dashed lines, respectively. Reprinted with permission from [6].

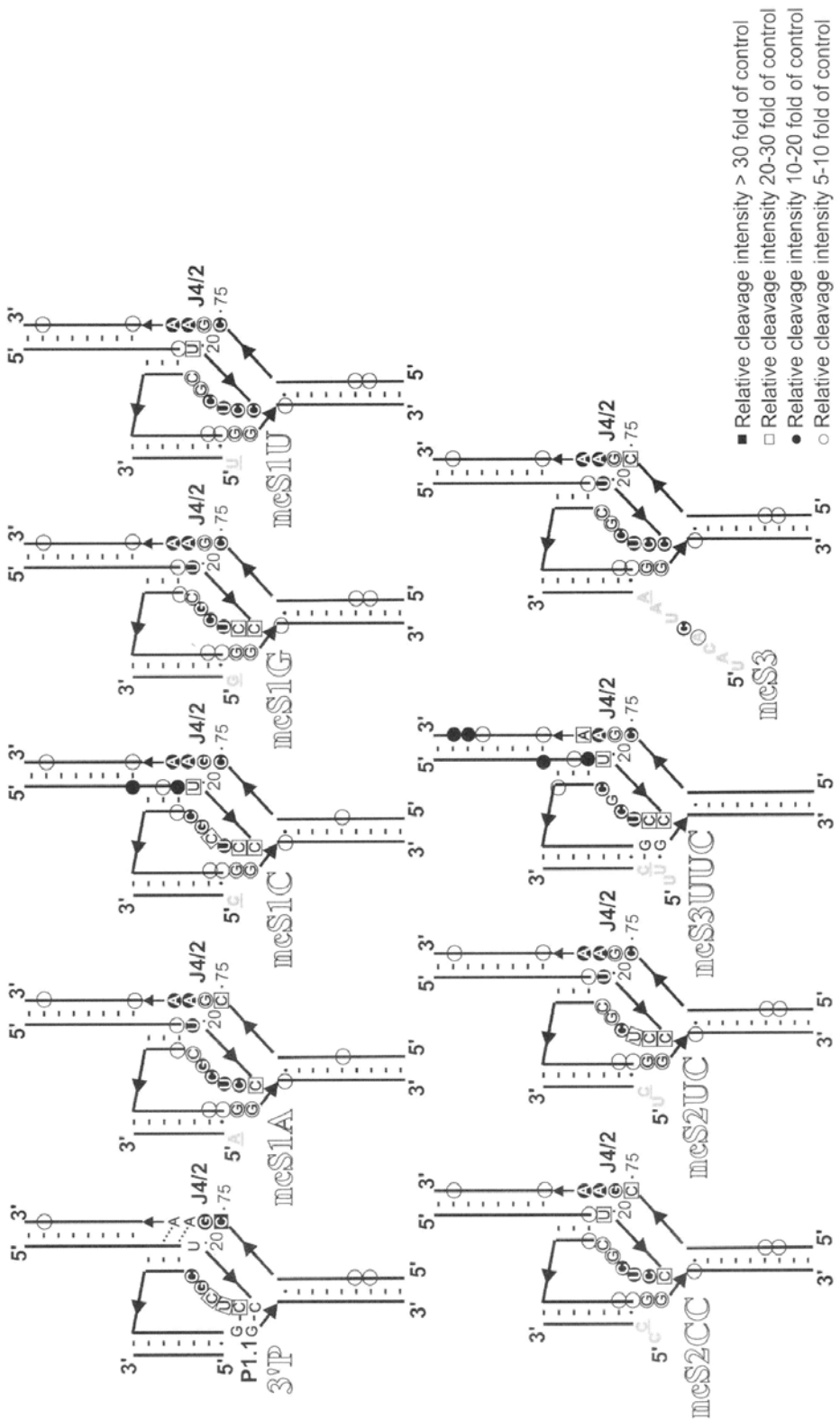
■ Relative cleavage intensity > 30 fold of control
□ Relative cleavage intensity 20-30 fold of control
● Relative cleavage intensity 10-20 fold of control
○ Relative cleavage intensity 5-10 fold of control
3'P
mcS1A
mcS1C
mcS1G
mcS1U
mcS2CC
mcS2UC
mcS3UUC
mcS3
P1.1
J4/2

change occurs upon HDV ribozyme catalysis and 5′ product dissociation from the 3′ product [6].

While previous evidence from fluorescence resonance energy transfer [8], 2-aminopurine fluorescence quenching [9] and NMR spectroscopy [10, 11] had already hinted at structural differences between the precursor and 3′ product forms of the *trans*-acting HDV ribozyme, terbium(III)-mediated footprinting complements these techniques by providing specifics of these rearrangements at nucleotide resolution. Particularly intriguing are the differences in the catalytic core structure around C75 and P1.1 that may control access to the cleavage transition state and may therefore explain differences in the catalytic rate constants for substrates with different 5′ sequences (Fig. 12.2) [6]. In fact, the 5′ substrate sequence subtly modulates the terbium(III) footprinting pattern, but all the substrates consistently show strong cuts in the P1.1 stem and the ribose zipper motif of J4/2 (Fig. 12.2). This implies that in the precursor these tertiary structure interactions are not fully formed, in contrast to the 3′P complex. Interestingly, these subtle differences in the catalytic core structure of the various precursor complexes translate into significant changes in fluorescence resonance energy transfer (FRET) efficiency between fluorophores attached to the termini of P4 and P2 stems [6]. Taken together, these results indicate that the various precursor complexes differ in structure both locally (in the catalytic core) and globally (as measured by FRET), providing an explanation for the wide range of catalytic activities of substrates with varying 5′ extensions [6, 12].

Several other labs have also found terbium(III) to be a useful probe of high-affinity metal binding sites and tertiary structure in RNA. Musier-Forsyth and coworkers were able to show that terbium substitutes for several well known metal binding sites in human $tRNA^{Lys,3}$ and works as a sensitive probe of tertiary structure. At low Tb^{3+} concentrations, cleavage of $tRNA^{Lys,3}$ is restricted to nucleotides that were previously identified from X-ray crystallography as specific metal-binding pockets [13]. The use of higher Tb^{3+} concentrations resulted in an overall footprint of the L-shaped tRNA structure, showing increased cleavage in the loop regions (D and anticodon loops). Binding of HIV nucleocapsid protein could then be shown to result in the disruption of the tRNA's metal binding pockets and, at higher concentrations, to induce subtle structural changes in, for example, the tRNA acceptor–TψC stem minihelix [14]. Other RNAs that have similarly been studied by terbium(III)-mediated footprinting include the hammerhead [15], aminoacyl-transferase [16, 17], RNase P [18] and group II intron ribozymes [19].

12.4 Troubleshooting

Initial titration experiments will be necessary to obtain the optimal Tb^{3+} concentration(s) to use for structure probing of any individual RNA [typical terbium(III) and RNA concentrations for determining tertiary structural features are around 1–5 mM and 1 μM, respectively]. The trivalent terbium(III) has been shown to induce

slight perturbations in the RNA structure [13], but careful titration will reveal the optimal terbium(III):RNA ratio needed for detecting unbiased secondary and tertiary structure features in a given RNA molecule.

To verify a high-affinity metal-ion-binding site, it is advisable to first decrease the Tb^{3+} concentration until a very narrow cleavage pattern is observed (typically at 10–100 μM Tb^{3+}) and then to perform a competition experiment with increasing concentrations of Mg^{2+}. The intensity (or fraction of RNA cleaved at a particular nucleotide position) should decrease as the Mg^{2+} concentration increases. Quantifying the intensities of cleaved bands at each nucleotide position directly relates to the structure of the RNA. It is critical to keep the extent of total cleavage lower than 20% of the uncleaved or full-length band. This will ensure that the RNA is undergoing a single cleavage event. Finally, it is important to keep in mind that, while terbium(III) footprinting will reveal many high-affinity metal ion binding sites, it may not reveal all. This is due to the fact that there is a steric requirement of Tb^{3+} to bind close to the 2′-hydroxyl group on the ribose for inducing backbone cleavage. This restraint is very unfavorable in A-type RNA helices and, therefore, strong metal sites that occur in RNA helical regions may be underestimated or go undetected by Tb^{3+} cleavage, as may binding sites that are highly specific for a particular metal ion [19].

References

1 Pyle, A. M. *J. Biol. Inorg. Chem.* **2002**, *7*, 679–690.

2 Ciesiolka, J., T. Marciniec, W. Krzyzosiak. *Eur. J. Biochem.* **1989**, *182*, 445–450.

3 Walter, N. G., N. Yang, J. M. Burke. *J. Mol. Biol.* **2000**, *298*, 539–555.

4 Baes, C. F., R. E. Mesmer. *The Hydrolysis of Cations*, Wiley Interscience, New York, **1976**.

5 Matsumura, K., M. Komiyama. *J. Biochem.* **1997**, *122*, 387–394.

6 Jeong, S., J. Sefcikova, R. A. Tinsley, D. Rueda, N. G. Walter. *Biochemistry* **2003**, *42*, 7727–7740.

7 Hadziyannis, S. J. *J. Gastroenterol. Hepatol.* **1997**, *12*, 289–298.

8 Pereira, M. J., D. A. Harris, D. Rueda, N. G. Walter. *Biochemistry* **2002**, *41*, 730–740.

9 Harris, D. A., D. Rueda, N. G. Walter. *Biochemistry* **2002**, *41*, 12051–12061.

10 Luptak, A., A. R. Ferre-D'Amare, K. Zhou, K. W. Zilm, J. A. Doudna. *J. Am. Chem. Soc.* **2001**, *123*, 8447–8852.

11 Tanaka, Y., M. Tagaya, T. Hori, T. Sakamoto, Y. Kurihara, M. Katahira, S. Uesugi. *Genes Cells* **2002**, *7*, 567–579.

12 Shih, I., M. D. Been. *EMBO J.* **2001**, *20*, 4884–4891.

13 Hargittai, M. R., K. Musier-Forsyth. *RNA* **2000**, *6*, 1672–1680.

14 Hargittai, M. R., A. T. Mangla, R. J. Gorelick, K. Musier-Forsyth. *J. Mol. Biol.* **2001**, *312*, 985–997.

15 Feig, A. L., M. Panek, W. D. Horrocks, Jr, O. C. Uhlenbeck. *Chem. Biol.* **1999**, *6*, 801–810.

16 Flynn-Charlebois, A., N. Lee, H. Suga. *Biochemistry* **2001**, *40*, 13623–13632.

17 Vaidya, A., H. Suga. *Biochemistry* **2001**, *40*, 7200–7210.

18 Kaye, N. M., N. H. Zahler, E. L. Christian, M. E. Harris. *J. Mol. Biol.* **2002**, *324*, 429–442.

19 Sigel, R. K., A. Vaidya, A. M. Pyle. *Nat. Struct. Biol.* **2000**, *7*, 1111–1116.